JOURNAL OF MATERIALS SCIENCE 22 (1987) 2237–2247

# Influence of synthesis chemistry on alumina–zirconia powder characteristics

J. C. DEBSIKDAR*
*Battelle Columbus Division, Columbus, Ohio 43201-2693, USA*

$80Al_2O_3 \cdot 20ZrO_2$ (wt%) powders were synthesized by three different chemical processes: (1) chemical polymerization, (2) destabilization of mixed sols, and (3) coprecipitation. The elementary particles produced by each of these processes were of the order of 1.5 to 3.0 nm and were amorphous to electron diffraction. The powders were evaluated in terms of (a) weight loss (thermal gravimetric analysis, TGA) and thermal (differential thermal analysis, DTA) characteristics, (b) surface area (BET), pore size distribution, and density at different temperatures; and (c) the crystallization behaviour (XRD method) which showed that the physiochemical characteristics and crystallization behaviour of these chemically derived powders are significantly influenced by the chemistry of powder synthesis. Moreover, the powders produced by the chemical polymerization and the colloidal processes retained the tetragonal phase of zirconia completely during cooling from 1600° C, but significant transformation of tetragonal to monoclinic zirconia occurred in the coprecipitated powder under identical conditions. Furthermore, the 1550° C calcined powder derived by the chemical polymerization process retained a substantial amount of tetragonal zirconia after annealing at 1000° C for 72 h. The average alumina and zirconia crystal sizes of the calcined powders, calculated by the Scherrer formula, were in the 20 to 80 nm range.

## 1. Introduction

The development of methods for fabricating transformation-toughened ceramics, such as $Al_2O_3$–$ZrO_2$, spinel–$ZrO_2$, mullite–$ZrO_2$, $Si_3N_4$–$ZrO_2$ and others, has gained significant interest in recent years. Among these, zirconia-toughened alumina ceramics have been studied most widely. As a result of these studies, it has been recognized that in producing optimally tough transformation-toughened composite bodies the microstructure of the matrix material and the zirconia particles dispersed in the matrix must fulfil certain "design criteria" [1]. These criteria include retention of zirconia particles with tetragonal symmetry in the fine-grained ceramic matrix. Moreover, the fabrication process parameters should be such that both size and size distribution of zirconia particles should be very small and that these particles are homogeneously distributed in the matrix material. Therefore, preparation of optimum quality powder is extremely important for producing $Al_2O_3$–$ZrO_2$ or other transformation-toughened ceramics having optimum mechanical properties (strength and toughness).

Several methods of preparing $Al_2O_3$–$ZrO_2$ powders have been reported in the literature. The conventional methods involve either dry milling [2–5] or wet milling [6, 7] a mixture of commercially available $Al_2O_3$ and $ZrO_2$ powders. The main disadvantage of the conventional approach relates to inhomogeneous mixing in terms of particle spacing and, as a consequence, inhomogeneity of the ceramic microstructure. Heuer *et al.* [8] and others have used a modified approach which involves spray drying an aqueous slurry of $Al_2O_3$ and $ZrO_2$ to produce the composite powder. A further modification of this approach has involved using an aqueous slurry containing $Al_2O_3$ and a selected zirconium salt for spray drying [9, 10] or spray roasting (or evaporative decomposition) [11].

Aksay [12] reported an approach in which the particles of $Al_2O_3$ and $ZrO_2$ are mutually dispersed by controlling the pH of the aqueous medium at 2 to 3.5; the slurry thus produced is filtered through a gypsum mould to form the "green" composite body. This approach has been modified by Lange and Hirlinger [13] who dispersed $Al_2O_3$ and $ZrO_2$ particles separately in the aqueous medium in the pH range of 2 to 3, aged the suspensions for 24 h and collected all particles $\leqslant 1\,\mu m$ separately from each suspension by pH controlled sedimentation processes. Subsequently the flocced slurries were mixed in the desired proportion, redispersed at pH 2, again flocculated (at pH 8) and, finally, centrifuged to produce the "green" composite body. This approach may be expected to produce a more homogeneous microstructure of the final ceramic than that reported by Aksay [12].

Several investigators [4, 8, 14, 15] have used aqueous solutions (or sols) of aluminium and zirconium salts to produce powders by coprecipitation [4], spray drying [8, 14] or the so-called spray-ICP technique [15] which involves spraying the solution (or sol) in an inductively coupled plasma at 5000 K. The use of metal organic

* *Present address*: EG & G Idaho Inc., Idaho Falls, Idaho 83415, USA.

0022–2461/87 $03.00 + .12 

precursors (alkoxides) has also been reported [16, 17]. Fegley Jr. *et al.* [16] produced $Al_2O_3$–$ZrO_2$ composite powder by controlled hydrolysis of a nonaqueous slurry containing $Al_2O_3$ powder and a zirconium alkoxide in a dry $N_2$ atmosphere and centrifuging the resultant slurry. Pugar and Morgan [17] mixed the alkoxide precursors of $Al_2O_3$ and $ZrO_2$ in a non-aqueous medium and then hydrolysed the solution (or sol) in a controlled manner to effect polymerization reactions between the alkoxides, producing the desired $Al_2O_3$–$ZrO_2$ composite powder. Other methods, such as CVD [18] and directional solidification of eutectics [19, 20], have also been studied for producing $Al_2O_3$–$ZrO_2$ ceramic composites.

The main objective of the present investigation was to study the relationship between the chemistry of powder preparation and the mechanical properties and microstructure of $80Al_2O_3 \cdot 20ZrO_2$ composite ceramic. With this objective, composite powders were prepared by three chemically different routes. This paper presents a comparative evaluation of the characteristics of these powders.

## 2. Experimental procedure

### 2.1. Powder preparation

$80Al_2O_3 \cdot 20ZrO_2$ (wt %) powders were prepared using commercially available reagent-quality chemicals (Morton Thiokol, Inc., Alfa Products, Danvers, Massachusetts, USA); namely, aluminium sec butoxide, $Al(OC_4H_9)_3$ (95%); aluminium isopropoxide, $Al(O_3H_7)_3$ (98.5%); aluminium nitrate, $Al(NO_3)_3 \cdot 9H_2O$; zirconium n-propoxide, $Zr(OC_3H_7)_4$ containing 21.6 g zirconium per 100 ml and zirconium dinitrate oxide, $ZrO(NO_3)_2 \cdot XH_2O$ containing 40.1% $ZrO_2$. Powders were prepared by three different processes based on three different chemical principles; namely, a process based on chemical polymerization between $Al(OC_4H_9)$ and $Zr(OC_3H_7)_4$ (hereafter referred to as Procedure 1); a process based on destabilization of a mixed sol (the so-called colloid chemistry approach) prepared from $Al(OC_3H_7)_3$ and $ZrO(NO_3)_2 \cdot XH_2O$ (Procedure II), and the coprecipitation process using a solution mixture of $Al(NO_3)_3 \cdot 9H_2O$ and $ZrO(NO_3)_2 \cdot XH_2O$ (Procedure III).

#### 2.1.1. Procedure I

406.9 g aluminium sec butoxide, $Al(OC_4H_9)_3$ was dissolved in 500 ml 1-butanol containing 75 ml acetylacetone. The clear solution thus obtained was partially hydrolysed by adding 230 ml distilled water/ethanol mixture (30 ml distilled water + 200 ml anhydrous ethanol) and stirring for 1 h in the ambient environment. Subsequently, 68.6 ml zirconium n-propoxide was added and stirred for 2 h; a clear (brownish) solution resulted. Finally, 500 ml water/ethanol mixture (water : ethanol ratio approximately 1 : 2 by vol) was added in a continuous stream under vigorous stirring. The resultant clear (brownish) solution (pH < 7) formed a transparent brown gel overnight in an air oven at 70° C. A small amount of the material was set aside for study of its microstructure and crystallinity and the rest was dried in an air oven at 110° C for a week, then milled for 3 h in a plastic bottle using alumina balls to produce the powder.

#### 2.1.2. Procedure II

An alumina sol was prepared by first precipitating 325.4 g aluminium isopropoxide, $Al(OC_3H_7)_3$, in hot (70° C) distilled water and then peptizing the precipitate with 9 ml concentrated nitric acid, $HNO_3$, for approximately 5 h at the same temperature. A clear sol (2000 ml) was obtained. The volume of this sol was reduced to about 1000 ml by evaporation. Simultaneously, an aqueous sol of zirconia (500 ml) was prepared (at pH 4) using 49.88 g zirconium dinitrate oxide, $ZrO(NO_3)_2$. Subsequently, the sols were mixed and treated with $NH_4OH$/water mixture ($NH_4OH$: water ratio approximately 1 : 10 by vol). A slightly translucent gel was obtained at (pH < 6) at the ambient temperature. The gel was dispersed in distilled water and centrifuged three times to remove the nitrate ($NO_3^-$) ions. A small amount of the washed material was set aside for study of its microstructure and crystallinity and the rest dried in an air oven at 110° C for a week, then milled in a plastic bottle for 3 h using alumina balls to produce the powder.

#### 2.1.3. Procedure III

An aqueous solution (total volume 1100 ml) containing 453.59 g aluminium nitrate, $Al(NO_3)_3 \cdot 9H_2O$ and 38.43 g zirconium dinitrate oxide, $ZrO(NO_3)_2 \cdot XH_2O$ was treated with concentrated $NH_4OH$ at ambient temperature under vigorous stirring. A white voluminous precipitate was formed at pH 8 to 10. After allowing the precipitate to settle overnight the supernatant liquid was decanted. The precipitate was dispersed (in distilled water) and centrifuged three times. A small amount of the washed material was set aside for microstructural and crystallinity study and the rest was dried in an air oven at 110° C for a week, then milled in a plastic bottle for 3 h using alumina balls to produce the powder.

### 2.2. Powder characterization

The microstructure and selected area electron diffraction pattern of the powder were examined using a JEOL JEM 100B scanning transmission electron microscope (Jeol, Inc, Peabody, Massachusetts) operated at 80 kV. The specimens were prepared using a drop of ultrasonically dispersed (in anhydrous ethanol) suspension on a carbon-coated grid.

Weight loss and thermal characteristics were examined by thermal gravimetric (TGA) and differential thermal (DTA) methods, respectively. For both TGA and DTA, the samples were heated in a free-flowing oxygen atmosphere at 50° C $h^{-1}$.

BET surface area, total pore volume, average pore radius, and pore size distribution of the powders were determined on an automatic volumetric sorption analyser (AUTOSORB-6, Quantachrome Corp., New York) using nitrogen as the absorbate. These measurements were made on 110° C dried and 500° C heat-treated Procedure I, II, and III powders and, in addition, on 850° C and 1050° C heat-treated Procedure I powder.

The true density of the powders heat-treated at 500, 850, 1050 and 1200° C was measured on a pycnometer (Penta-Pycnometer, Quantachrome Corp., New York) using helium as the displacement fluid.

X-ray diffraction (XRD) analyses were conducted on a computer-controlled Rigaku diffractometer having a peak search attachment. Procedure I, II, and III powders heated for 2 h each at 400 and 1000° C, and those obtained after DTA (1600° C) were used to study the phase composition. Additionally, XRD analysis was done on the 1550° C heat-treated Procedure I powder which was annealed at 1000° C for 72 h during the cooling cycle. The crystal size of the heat-treated powders was determined by the Scherrer formula (crystal size $= 0.9\lambda/(B \cos \theta)$, where $\lambda = 1.5405$, $B$ = width at the half-peak height in radians, and $\theta$ = Bragg angle).

## 3. Results and discussion

### 3.1. Powder synthesis

The synthesis of the Procedure 1 powder involved a controlled hydrolysis of $Al(OC_4H_9)_3$ and $Zr(OC_3H_7)_4$ to allow polymerization reactions. Because these alkoxides are very sensitive to moisture (on exposure to moisture they quickly form powdery materials which may have complex molecular structures) a special environment is often necessary [16] to effectively control their hydrolysis. However, this situation can be avoided if these alkoxides are treated with a complexing agent prior to hydrolysis [21, 22]. In this synthesis procedure a clear solution of $Al(OC_4H_9)_3$ was prepared in 1-butanol in the presence of acetylacetone as a complexing agent and the polymerization reactions between $Al(OC_4H_9)_3$ and $Zr(OC_3H_7)_4$ carried out without requiring a special environment. The polymer network formed by hydrolytic polycondensation reactions extended throughout the liquid medium, thickening it to a gel.

The synthesis of the Procedure II powder involved the following steps: preparation of stable $Al_2O_3$ and $ZrO_2$ (hydrous) sols, mixing these sols, and finally, destabilizing the mixed sols. In this case the surface charges (of the particles in the mixed sol) that determined the net repulsion effect were reduced by adding ammonium hydroxide to form the gel.

The coprecipitation (Procedure III) involved separating the insoluble molecular aggregate of the hydrous oxides of aluminium and zirconium from the solvent, as a result of the interaction between the ions present in the solution (or sol). Precipitation is a complex uncontrollable process composed of reaction mechanisms that include polymerization, particle growth, and aggregation [23].

### 3.2. Microstructure and crystallinity

The TEM micrographs were taken at a very high magnification (300 K) because the microstructure of the as-prepared materials could not be resolved at a lower magnification. Figs 1, 2 and 3 show the TEM micrographs of the Procedure I, II and III materials, respectively. The microstructure of the Procedure I material showed round particles. The microstructures of the Procedure II and III materials appeared stringy; however, on a closer look, the elementary particles were found to be mostly round. On a rough estimate the particle sizes (Procedures I, II, and III) were in the 1.5 to 3.0 nm range. It may be noted here that during the TEM observations the material shrunk substantially due to the heat generated by the electron beam. Therefore, the particle sizes as seen in the TEM micrographs may not be representative of the as-prepared materials.

The selected area electron diffraction pattern of these materials (insets on the respective TEM micrographs) gave only diffused lines which imply that the as-prepared materials were amorphous.

### 3.3. Weight loss behaviour

The TGA curves of the Procedure I, II, and III powders (Figs 4 to 6) showed a total 36.5, 10.1 and 26.5% weight losses, respectively. The weight loss of Procedure I and II powders occurred in two distinctly different temperature ranges, one up to about 500° C, and the other between 500 and 900° C. The losses up to about 500° C which may be attributable to physical and chemisorbed water, and organics (if any) were 35.3 and 9.7%, respectively, for the Procedure I and II powders. On the other hand, the Procedure III powder lost weight continually up to 900° C.

Procedure I powder contained a substantial amount of organics, as evident in its DTA curve (Fig. 7). They may be due to the presence of residual organic solvent and/or residual alkoxy groups bound to the aluminium and/or zirconium atoms. They could be substantially removed by humidification of the gel prior to drying [24]. In addition to the physical and chemisorbed water, the Procedure II powder may contain some nitrate ($NO_3^-$) ions that are expected to be removed below 500° C. Beyond 500° C a further weight loss occurred with Procedure I and II powders (amounting to 1.2 and 0.4%, respectively) which may be due to the loss of structural water (decomposition of structural –OH groups). The Procedure III powder, which is a complex mixture of the hydrous oxides of aluminium and zirconium, lost water continually (although at different rates). In this case any nitrate ions, if present, would be expected to go off at lower temperature. Thus, the TGA results show that the magnitude and the nature of the weight loss for Procedure I, II, and III powders were significantly different.

### 3.4. Thermal behaviour

The thermal behaviours of the Procedure I, II, and III powders, as revealed by DTA, are shown in Figs 7, 8 and 9, respectively. The Procedure I powder (Fig. 7) gave an endothermic band at 70 to 300° C corresponding to the loss of physical and chemisorbed water, a sharp exothermic peak at 350° C resulting from the organic burnout, and a very broad low intensity exothermic band beyond 1000° C which perhaps is related to the processes involving pore closure and growth of crystals. The Procedure II and III powders did not give any exothermic peak around 350° C like the Procedure I powder; instead, the Procedure II powder gave an endothermic peak at 350° C (Fig. 8),

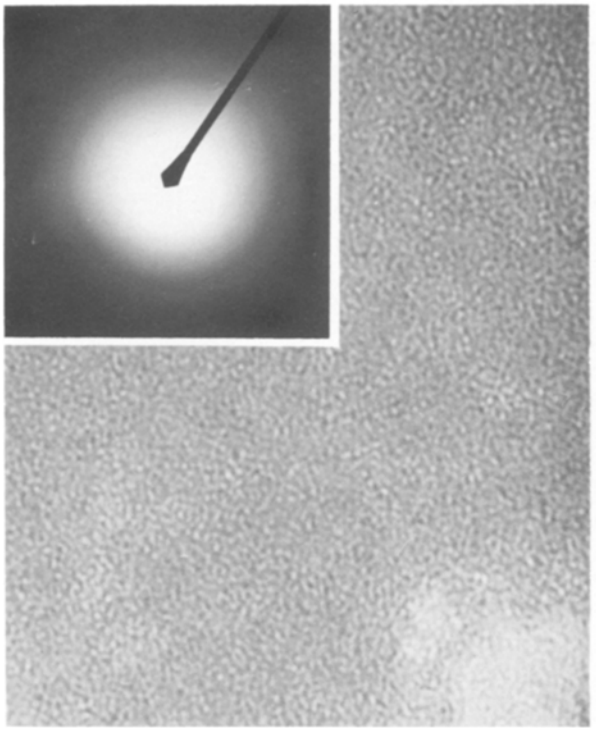

*Figure 1* TEM micrograph of Procedure I material. Inset: selected area electron diffraction pattern.

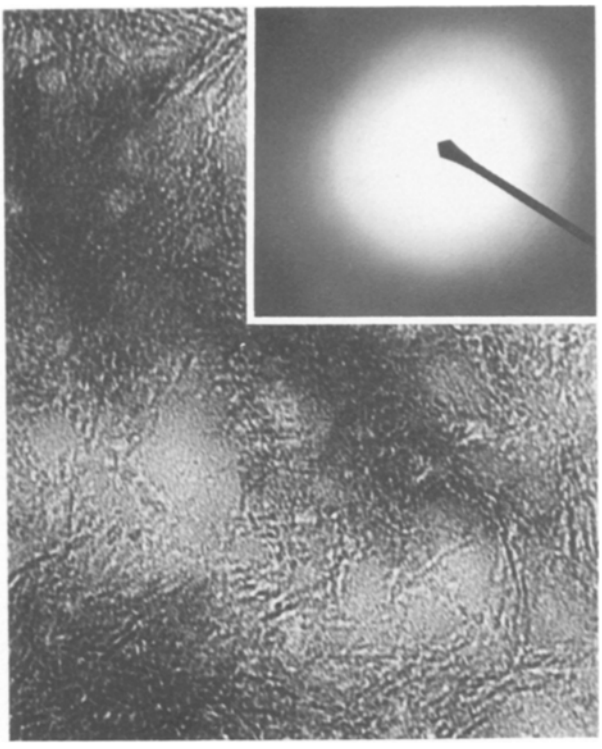

*Figure 2* TEM micrograph of Procedure II material. Inset: selected area electron diffraction pattern.

and Procedure III powder gave two well-defined but overlapping endothermic peaks at 340 and 460° C (Fig. 9), respectively. While the endothermic peak for the Procedure II powder may represent loss of the chemisorbed water, the situation with the Procedure III powder is different because it is constituted of the molecular aggregates of the hydrous oxides of aluminium and zirconium (plus some heterocondensation product). Therefore this powder is expected to lose water at different temperatures corresponding to the decomposition temperatures of those hydrous oxides. Since the decomposition temperature of aluminium hydrous oxide is lower than that of zirconium hydrous oxide, the peaks at 340 and 460° C may represent the maximum rate of decomposition of aluminium and zirconium hydrous oxides, respectively.

An exothermic peak corresponding to the crystallization process was not distinguishable in any of the DTA curves. The reason for this (as will be seen later) is that all these powders crystallized at less than 400° C (the region where thermal change(s) took place due to organic burnout and/or loss of water), consequently, the crystallization temperature(s) of these powders could not be identified from the respective DTA curves. However, the TGA and DTA results were consistent.

### 3.5. Surface area and pore structure

Multipoint BET surface area, pore volume, pore size (with maximum pore volume), and average pore size of the initial and heat-treated powders are shown in Table I. (The term pore size is used here as a synonym for pore radius.) The pore size distribution of the

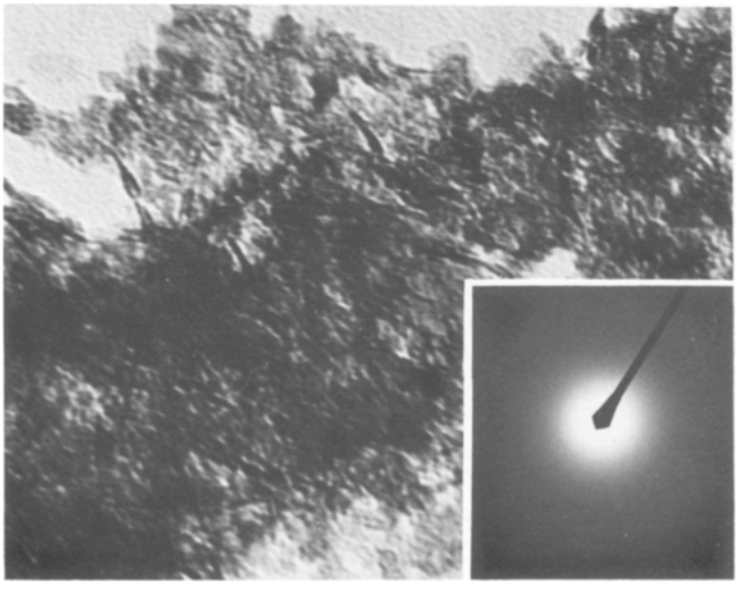

*Figure 3* TEM micrograph of Procedure III material. Inset: selected area electron diffraction pattern.

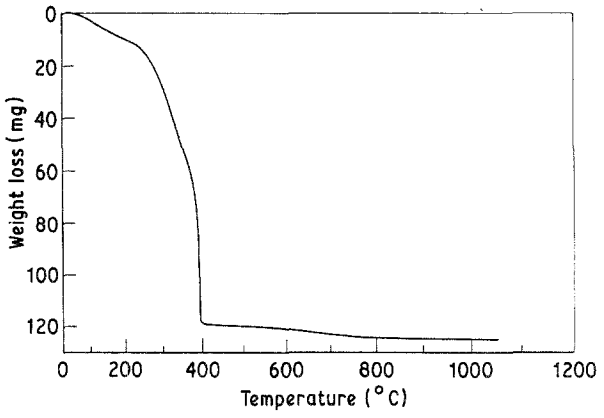


*Figure 4* TGA of Procedure I powder. Sample size, 328.8 mg; heating rate, 50° C $h^{-1}$.

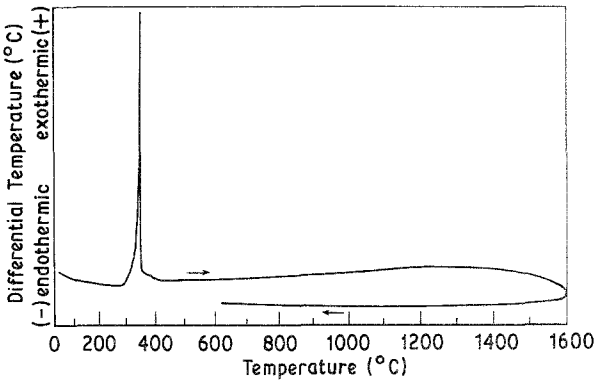


*Figure 7* DTA of Procedure I powder. Sample size, ~400 mg; heating rate, 50° C $h^{-1}$; cooling rate, 300° C $h^{-1}$.

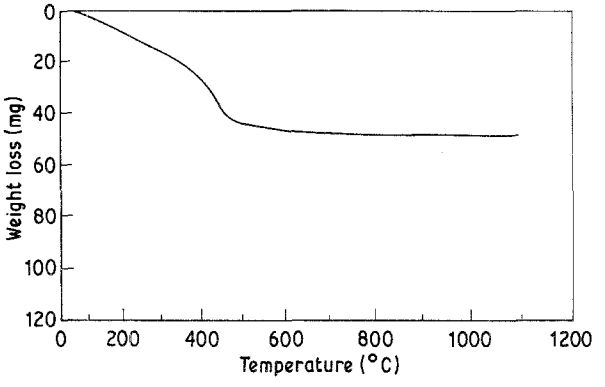


*Figure 5* TGA of Procedure II powder. Sample size, 487.2 mg; heating rate, 50° C $h^{-1}$.

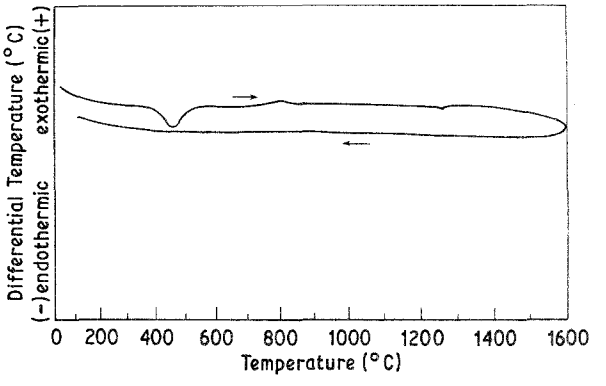


*Figure 8* DTA of Procedure II powder. Sample size, ~400 mg; heating rate, 50° C $h^{-1}$; cooling rate, 300° C $h^{-1}$.

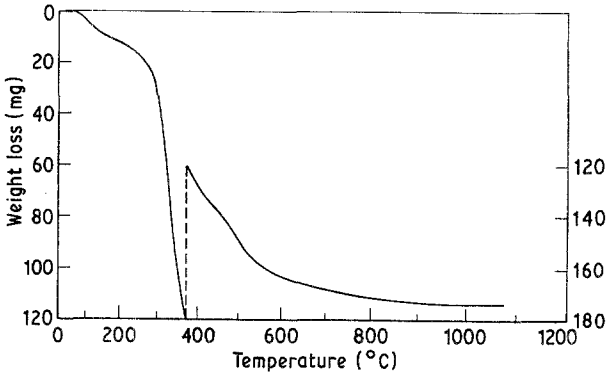


*Figure 6* TGA of Procedure III powder. Sample size, 658.0 mg; heating rate, 50° C $h^{-1}$.

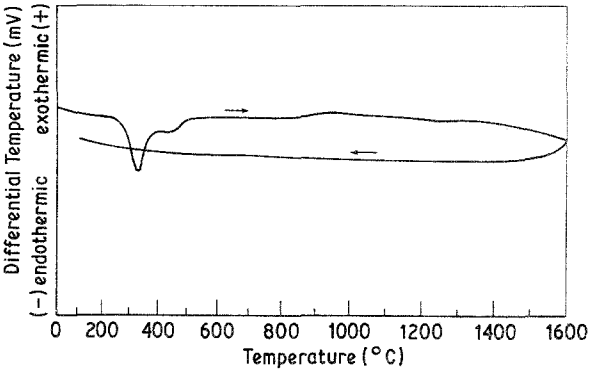


*Figure 9* DTA of Procedure III power. Sample size, ~400 mg; heating rate, 50° C $h^{-1}$; cooling rate, 300° C $h^{-1}$.

TABLE I Surface area, pore volume, pore size, and pore size distribution of Procedure I, II, and III powders heated at different temperatures

| Procedure | Heat Treatment | | Surface area ($m^2 g^{-1}$) | Pore volume ($cm^3 g^{-1}$) | Pore radius (cm × $10^{-8}$) | |
|---|---|---|---|---|---|---|
| | Temperature (° C) | Time (h) | | | Radius with maximum pore volume | Average |
| I | 110 | ~280 | 480 | 0.35 | 11.8 or less | 14.5 |
| | 500 | 2 | 218 | 0.39 | 22 | 28.3 |
| | 850 | 2 | 176 | 0.35 | 31 | 39.4 |
| | 1050 | 2 | 90 | 0.20 | 31.5 | 44.9 |
| II | 110 | ~280 | 325 | 0.49 | 31 | 29.9 |
| | 500 | 2 | 208 | 0.10 | 11.5 or less | 18.1 |
| III | 110 | ~280 | 357 | 0.39 | 18.5 | 21.6 |
| | 500 | 2 | 308 | 0.71 | 31 | 46.2 |

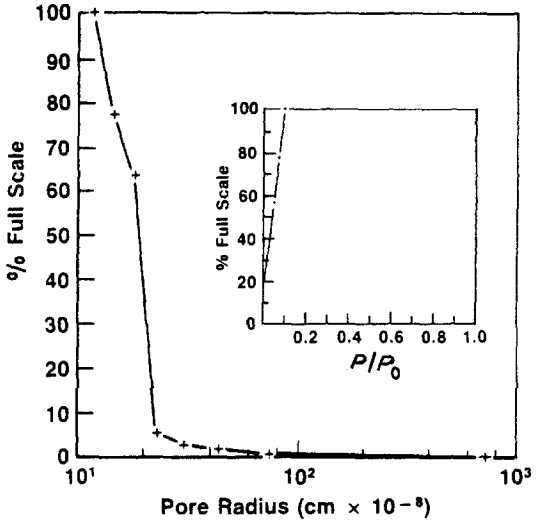


*Figure 10* Pore size distribution of Procedure I powder.

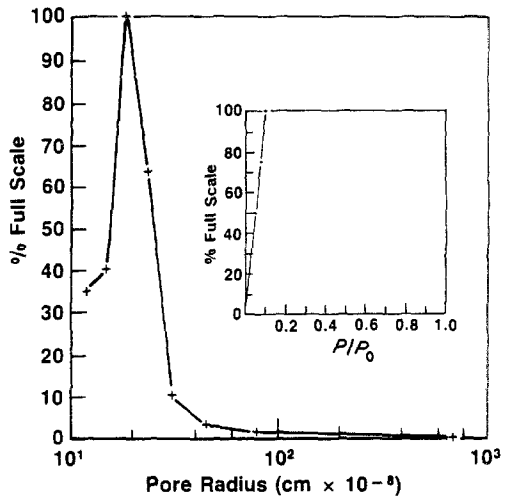


*Figure 12* Pore size distribution of Procedure III powder.

Procedure I, II, and III powders are shown in Figs 10, 11, and 12, respectively, and Figs 13 to 15 show the change of pore size distribution of the respective powders after heat treatment at higher temperatures. In these figures, the derivative of the cumulative pore volume with respect to radius ($dv/dr$) has been plotted against pore radius from the desorption isotherms.

The surface area of the Procedure I powder ($480\,m^2/g^{-1}$) was significantly larger than the corresponding Procedure II ($325\,m^2/g^{-1}$) and III ($357\,m^2g^{-1}$) powders. It must be noted here that the TEM micrographs (Figs 1 to 3) did not show any significant size difference of the elementary particles of the as-prepared Procedure I, II, and III materials. It is, therefore, anticipated that the differences in the BET surface area of these powders reflects, at least to some extent, the differences in the rate of particle growth during drying. The total pore volume of the Procedure I dried powder ($0.35\,cm^3g^{-1}$) was less than that for the corresponding Procedure II ($0.49\,cm^3g^{-1}$) and III ($0.39\,cm^3g^{-1}$) powders. These values appear to be consistent because the surface area data indicate that the Procedure I powder had the smallest particles among the three powders and the Procedure II powder the largest. The pore sizes (with maximum pore volume) were $12 \times 10^{-8}$, $31 \times 10^{-8}$, and $19 \times 10^{-9}$ cm, respectively, for the Procedure I, II, and III powders. The average pore size of these powders also showed a similar trend.

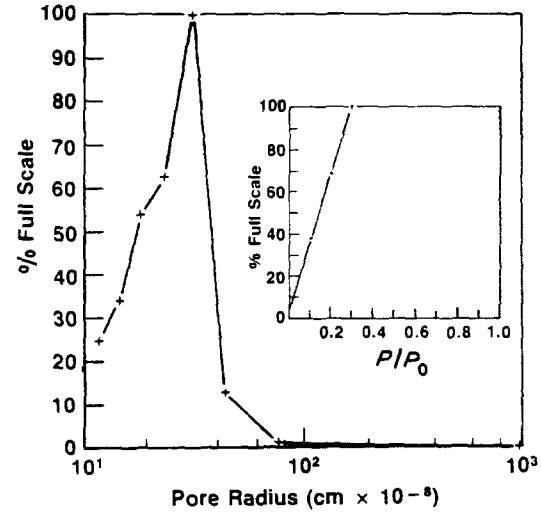


*Figure 11* Pore size distribution of Procedure II powder.

The pore size distribution of the powders varied. Almost the entire porosity of the Procedure I powder consisted of pores less than $23 \times 10^{-8}$ cm (Fig. 10), those of the Procedure II and III powders consisted of pores in the range 15 to $44 \times 10^{-8}$ cm (Fig. 11) and 15 to $30 \times 10^{-8}$ cm (Fig. 12), respectively.

When these powders were heated to 500° C, the surface areas decreased as expected but they showed significant differences in the change of the pore volume, pore size and pore size distribution. With the Procedure I powder, the pore volume increased to $0.39\,cm^3g^{-1}$, the pore size (the maximum pore volume) doubled (Table I), and the entire porosity now occurred in a very narrow size range, 10 to $20 \times 10^{-8}$ cm pore (Fig. 13b). The increase in pore volume and enlargement of the pores may be related to the evolution of chemisorbed water and organic burnout (Figs 4 and 7). It is, however, quite probable that at least some of the fine pores in the dried powder closed during this heat treatment. Furthermore it is interesting to note that the pore size further increased and the pore size distribution range shifted to higher values when the powder was heated to 850° C (Fig. 13c) which is related mostly to the loss of the structure water (i.e., structural –OH groups) from the powder (Fig. 4). Whether this increase of pore size and pore size range is related to bursting of the closed pores (containing structural water or other gases) [25, 26] is not clearly understood. A further increase of the heat-treatment temperature up to 1050° C did not produce any significant change in pore structure of this powder (Fig. 13d). The above results would indicate that a higher heat-treatment temperature is needed to make the Procedure I powder pore free.

The change of pore structure of the Procedure II and III powders was monitored only up to 500°C (Figs 14 and 15). With the Procedure II powder (Fig. 14), the pore size decreased and the entire porosity consisted of pores $< 23 \times 10^{-8}$ cm (against 15 to $44 \times 10^{-8}$ cm, before heat treatment), even though

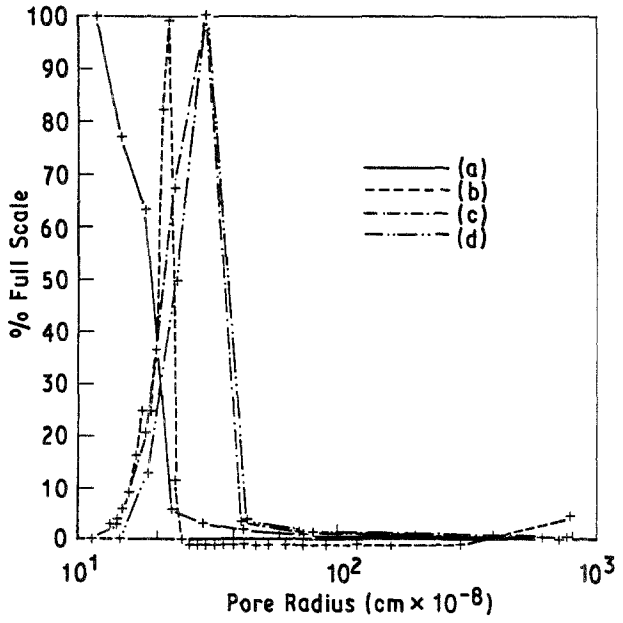


*Figure 13* Pore size distribution of Procedure I powder after different heat treatments. (a) 110° C, (b) 500° C, (c) 850° C and (d) 1050° C.

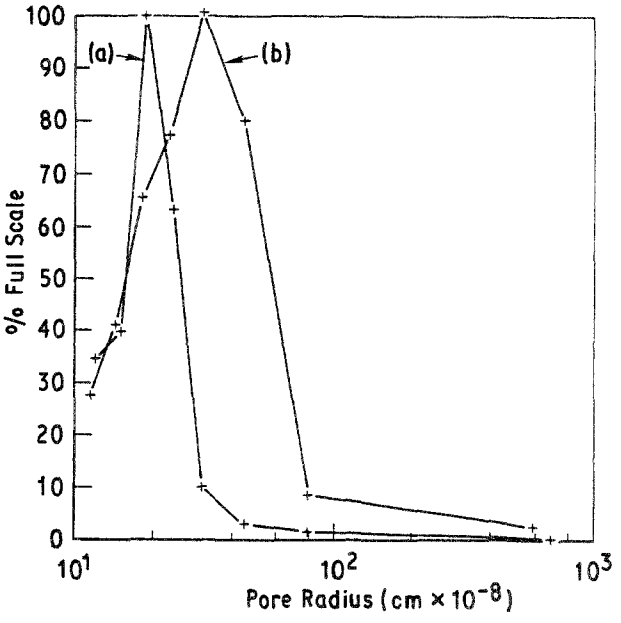


*Figure 15* Pore size distribution of Procedure III powder after different heat treatments. (a) 110° C, (b) 500° C.

some large pores still remained. Pore enlargement due to loss of the chemisorbed water (Fig. 5) was not evident in this case; on the contrary, a significant amount of pore closing took place during the 500° C heat treatment. A plausible explanation may be that since the pore size of this powder was initially larger than that of the Procedure I and II powders (see Table I) and also because the burning of organics was not involved (Fig. 8), pore enlargement did not occur during evolution of the chemisorbed water, and evidently the pore closing process was predominant. On the other hand, when the Procedure III powder was heated to 500° C, the pore size increased from 19 × $10^{-8}$ cm (before heat treatment) to 31 × $10^{-8}$ cm and the pore size range changed to 11 to 80 × $10^{-8}$ cm, from 15 to 30 × $10^{-8}$ cm (Fig. 15). In this case, pore enlargement appeared to be the dominant process over pore closing during the 500° C heat treatment.

In summary, the pore structure of the heat-treated powders was found to be related to the thermochemical reactions that occurred during the heat treatment and, in turn, to their synthesis chemistry.

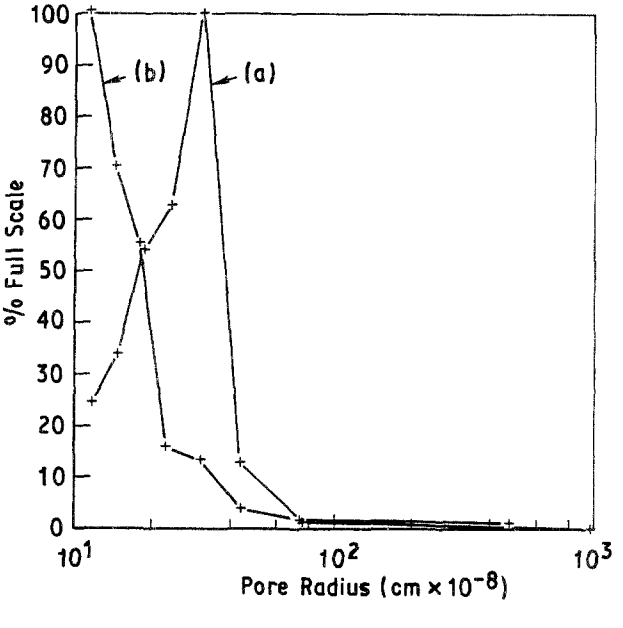


*Figure 14* Pore size distribution of Procedure II powder after different heat treatments. (a) 110° C, (b) 500° C.

## 3.6. Powder density

The progressive densification of the powders at increasingly higher temperatures, as determined on a helium pycnometer, can be seen from the data in Table II. Evidently, the as-prepared material in all cases had a much lower density than the theoretical, perhaps due to the structural disorder and the presence of anionic and other impurities. On heat treatment, progressive densification of the structural skeleton occurred due to capillary contraction, condensation polymerization, and structural relaxation [27]. The Procedure I powder fully densified at 1200° C or less. Even though Procedure II and III powders fully crystallized at this temperature, their densities were slightly lower than that of the Procedure I powder (Table II). It is tentatively presumed that the presence of minor impurities and/or some experimental error contributed to these lower values. Moreover, the Procedure III powder contained (as will be seen later) some amount of the monoclinic phase of $ZrO_2$, thus its density would be expected to be a little lower than that of the Procedure II powder which contained only tetragonal $ZrO_2$. This was indeed the case (Table II).

## 3.7. Crystallization behaviour

All three powders crystallized to a $\gamma$-$Al_2O_3$ structure at 400° C or less (Fig. 16) with crystal sizes 5.7, 7.9 and 8.6 nm (Table III), respectively, for the Procedure I, II, and III powders. At 1000° C, a partial transformation of $\gamma$-$Al_2O_3$ → $\theta$-$Al_2O_3$ occurred and tetragonal phase $ZrO_2$ (t-$ZrO_2$) precipitated out in the Procedure II and III powders; but the Procedure I powder contained only the $\gamma$-$Al_2O_3$ and t-$ZrO_2$ (Fig. 17). Thus, the

TABLE II Helium density of Procedures I, II, and III powders after heat treatment at different temperatures

| Procedure | Heat treatment | | Density ($g\,cm^{-3}$) | Percentage (theoretical)* |
|---|---|---|---|---|
| | Temperature (° C) | Time (h) | | |
| I | 500 | 2 | 3.35 | 77.9 |
| | 850 | 2 | 3.65 | 84.9 |
| | 1050 | 2 | 4.02 | 93.5 |
| | 1200 | 2 | 4.32 | 100.0 |
| II | 500 | 2 | 3.50 | 81.4 |
| | 850 | 2 | 3.68 | 85.6 |
| | 1050 | 2 | 3.97 | 92.3 |
| | 1200 | 2 | 4.20 | 97.7 |
| III | 500 | 2 | 3.52 | 81.9 |
| | 850 | 2 | 3.74 | 87.0 |
| | 1050 | 2 | 3.86 | 89.8 |
| | 1200 | 2 | 4.13 | 96.0 |

*Theoretical density of $80Al_2O_3 \cdot 20ZrO_2$ calculated by the method of mixture may be 4.3 or 4.2 depending on whether $ZrO_2$ is present with tetragonal or monoclinic symmetry, respectively. (Theoretical density assumed to be $4.3\,gm\,cm^{-3}$).

crystallization behaviour of the Procedure II and III powders generally conformed with that reported by Pugar and Morgan [17] for sol–gel derived $Al_2O_3$/10 vol % $ZrO_2$ powder; however, some differences were observed in the present investigation with respect to the rate of transformation of the $\gamma$-$Al_2O_3 \rightarrow \theta$-$Al_2O_3$ structure. With the Procedure II and III powders, $\gamma$-$Al_2O_3 \rightarrow \theta$-$Al_2O_3$ transformation was not complete at a temperature as high as 1000° C, whereas with the powder used by Pugar and Morgan, $\gamma$-$Al_2O_3$ transformed completely into $\theta$-$Al_2O_3$ structure at 900° C. Furthermore, with the Procedure I powder, the differences were even more significant. With the Procedure I powder, t-$ZrO_2$ precipitated out before the $\gamma$-$Al_2O_3 \rightarrow \theta$-$Al_2O_3$ transformation started (within the XRD detectability limit), whereas, according to Pugar and Morgan, [17], "$ZrO_2$ precipitates out during the $\gamma$-$Al_2O_3 \rightarrow \theta$-$Al_2O_3$ transformation". The differences in the crystallization kinetics (from those reported by Pugar and Morgan) perhaps indicate that the crystallization behaviour of the chemically derived $Al_2O_3$–$ZrO_2$ composites powders depends on their synthesis history, due to structural variations [28] as well as the composition ($Al_2O_3/ZrO_2$ ratio). Evidently, the powders used in the present investigation crystallized at a lower rate (than those used by Pugar and Morgan [17]). It is to be noted further that, among the powders used in the present investigation, the Procedure I powder crystallized at a lower rate than the Procedure II and III powders which can be seen from the nature of the diffraction peaks in Figs 16 and 17 and the crystal sizes (Table III).

The XRD data of the powders after DTA and those of the 1550° C heated and annealed (1000° C for 72 h) Procedure I powder are shown in Tables IV and V, respectively, and the crystal size distribution in Table

TABLE III Crystal size distribution in heat treated powders

| Procedure | Heat treatment | $Al_2O_3$ | | | $ZrO_2$ | | |
|---|---|---|---|---|---|---|---|
| | | Phase | hkl index | Crystal size (nm) | Phase* | hkl index | Crystal size (nm) |
| I | 400° C per 2 h, cooled naturally | $\gamma$ | 400 | 5.7 | – | – | – |
| | 1000° C per 2 h, cooled naturally | $\gamma$ | 400 | 6.3 | t | 111 | 6.3 |
| | 1600° C, cooled at 300° C per h (DTA) | $\alpha$ | 113 | 39.2 | t | 111 | 21.0 |
| | 1550° C per 2 h, annealed at 1000° C per 72 h, cooled naturally | $\alpha$ | 113 | 76.5 | t | 111 | 29.1 |
| | | | | | m | $11\bar{1}$ | 73.3 |
| II | 400° C per 2 h, cooled naturally | $\gamma$ | 400 | 7.9 | – | – | – |
| | 1000° C per 2 h, cooled naturally | $\gamma$ | 400 | 7.0 | t | 111 | 19.0 |
| | | $\theta$ | 202 | 18.4 | | | |
| | 1600° C, cooled at 300° C per h (DTA) | $\alpha$ | 113 | 39.2 | t | 111 | 26.1 |
| III | 400° C per 2 h, cooled naturally | $\gamma$ | 400 | 8.6 | – | – | – |
| | 1000° C per 2 h, cooled naturally | $\gamma$ | 400 | 8.2 | t | 111 | 11.3 |
| | | $\theta$ | 202 | 18.5 | | | |
| | 1600° C, cooled at 300° C per h (DTA) | $\alpha$ | 104 | 46.3 | t | | |
| | | | | | m | $11\bar{1}$ | 41.3 |

*t = tetragonal, m = monoclinc.

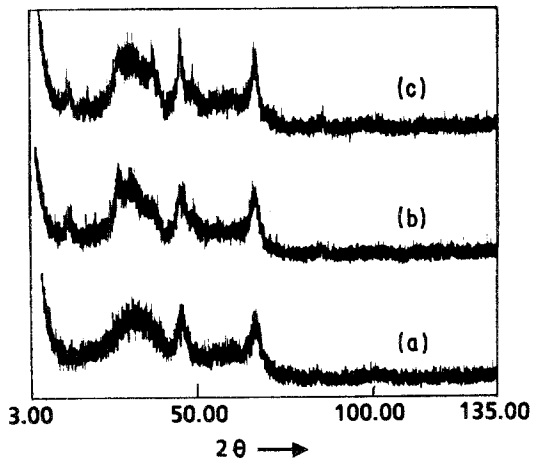


*Figure 16* X-ray diffraction pattern after 400° C heat treatment. (a) Procedure I, (b) Procedure II and (c) Procedure III.

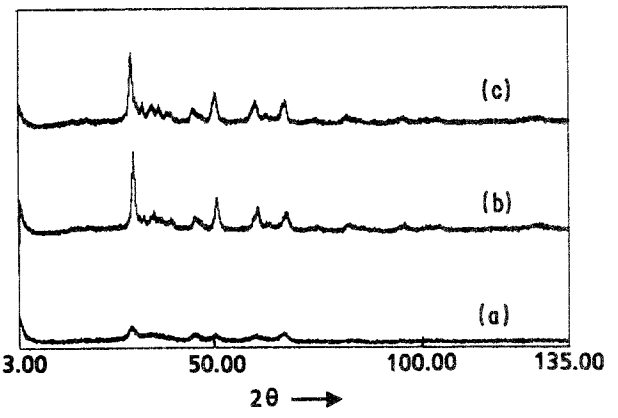


*Figure 17* X-ray diffraction pattern after 1000° C heat treatment. (a) Procedure I, (b) Procedure II and (c) Procedure III.

III. This study was conducted to examine the effect of the synthesis chemistry on the stability of the t-$ZrO_2$ in the monoclinic phase field. Both Procedure I and II powders retained the t-$ZrO_2$ phase fully after the DTA (cooling rate 300° C $h^{-1}$), but a partial t-$ZrO_2$ → m-$ZrO_2$ (monoclinic zirconia) transformation occurred in the Procedure III powder under the same conditions (Table IV). Moreover, the Procedure I powder after 1550° C heat treatment retained the t-$ZrO_2$ phase substantially during annealing at 1000° C for 72 h (Table V). The XRD results of the powders after DTA show that the stability of the t-$ZrO_2$ phase in the monoclinic phase field is influenced by the synthesis chemistry of the powder.

TABLE IV X-ray diffraction data for powders after heat treatment at 1600° C (Cu$K\alpha$ radiation)

| Procedure I | | | Procedure II | | | Procedure III | | |
|---|---|---|---|---|---|---|---|---|
| $d$(nm) | $1/1_0$ | Phase* | $d$(nm) | $1/1_0$ | Phase* | $d$(nm) | $1/1_0$ | Phase* |
| 0.3485 | 50 | α | 0.3482 | 39 | α | 0.5139 | 2 | M |
| 0.2964 | 100 | T | 0.2964 | 100 | T | 0.3687 | 6 | M |
| 0.2603 | 10 | T | 0.2595 | 10 | T | 0.3482 | 48 | α |
| 0.2559 | 51 | α, T | 0.2550 | 78 | α, T | 0.3166 | 29 | M, T |
| 0.2384 | 26 | α | 0.2380 | 26 | α | 0.2961 | 63 | T |
| 0.2091 | 37 | α | 0.2084 | 79 | α | 0.2839 | 20 | M |
| 0.1824 | 24 | T | 0.1822 | 25 | T | 0.2600 | 9 | M, T |
| 0.1821 | 32 | T | 0.1800 | 24 | T | 0.2553 | 91 | α |
| 0.1742 | 35 | α | 0.1740 | 30 | α | 0.2382 | 36 | α |
| 0.1603 | 66 | α, T | 0.1601 | 65 | α, T | 0.2209 | 4 | M |
| 0.1565 | 10 | α, T | 0.1561 | 14 | α, T | 0.2086 | 100 | α |
| 0.1559 | 7 | T | 0.1556 | 7 | T | 0.1845 | 6 | M |
| 0.1540 | 19 | T | 0.1537 | 31 | α | 0.1836 | 4 | T |
| 0.1512 | 7 | α | 0.1510 | 6 | α | 0.1814 | 26 | M |
| 0.1507 | 3 | α | 0.1408 | 7 | T | 0.1800 | 19 | M, T |
| 0.1479 | 6 | T | 0.1405 | 21 | α | 0.1742 | 34 | α |
| 0.1405 | 29 | α | 0.1374 | 37 | α | 0.1735 | 23 | α |
| 0.1402 | 14 | α | 0.1272 | 6 | α, T | 0.1692 | 3 | M |
| 0.1375 | 35 | α | 0.1240 | 7 | α | 0.1658 | 5 | M |
| 0.1274 | 5 | α, T | 0.1147 | 3 | α | 0.1601 | 90 | α, T |
| 0.1272 | 5 | α, T | 0.1125 | 3 | α | 0.1538 | 18 | M, T |
| 0.1239 | 13 | α | 0.1042 | 15 | α | 0.1516 | 3 | α |
| 0.1234 | 7 | α | 0.0909 | 4 | α | 0.1506 | 5 | α |
| 0.1231 | 4 | – | 0.0905 | 4 | α | 0.1478 | 7 | M |
| 0.1191 | 3 | α, T | | | | 0.1406 | 24 | α |
| 0.1179 | 6 | T | | | | 0.1401 | 17 | α |
| 0.1148 | 5 | α | | | | 0.1374 | 51 | α |
| 0.1099 | 5 | α | | | | 0.1272 | 5 | α, T |
| 0.1097 | 3 | – | | | | 0.1239 | 14 | α |
| 0.1079 | 6 | α | | | | 0.1235 | 10 | α |
| 0.1043 | 17 | α | | | | 0.1189 | 5 | α |
| 0.0998 | 10 | α | | | | 0.1179 | 5 | M, T |
| 0.0979 | 4 | α | | | | 0.1147 | 3 | α |
| 0.0908 | 8 | α | | | | 0.1078 | 7 | α |
| | | | | | | 0.1043 | 16 | α |
| | | | | | | 0.0998 | 12 | α |
| | | | | | | 0.0979 | 4 | α |
| | | | | | | 0.0908 | 8 | α |
| | | | | | | 0.0905 | 5 | α |

*α = Alpha alumina, T = tetragonal zirconia, M = monoclinic zirconia.

TABLE V X-ray diffraction data for 1550° C – 2 h heat treated Procedure I powder annealed at 1000° C for 72 h

| $d$(nm) | $I/I_0$ | Phase* |
|---|---|---|
| 0.5063 | 3 | M |
| 0.3678 | 6 | M |
| 0.3446 | 65 | α |
| 0.3151 | 28 | T, M |
| 0.2951 | 86 | T |
| 0.2827 | 18 | M |
| 0.2597 | 9 | T |
| 0.2545 | 99 | α, T |
| 0.2373 | 42 | α |
| 0.2103 | 3 | α |
| 0.2080 | 100 | α |
| 0.1843 | 4 | T |
| 0.1816 | 28 | M |
| 0.1799 | 12 | α |
| 0.1737 | 43 | α |
| 0.1732 | 23 | α |
| 0.1649 | 4 | M |
| 0.1599 | 86 | α, T |
| 0.1564 | 3 | α, T |
| 0.1535 | 20 | M, T |
| 0.1508 | 9 | α |
| 0.1479 | 6 | T |
| 0.1476 | 7 | M, T |
| 0.1403 | 31 | α |
| 0.1389 | 17 | α |
| 0.1373 | 31 | α, T |
| 0.1271 | 4 | α, T |
| 0.1238 | 13 | α |
| 0.1232 | 7 | α |
| 0.1229 | 5 | – |
| 0.1188 | 5 | α |
| 0.1178 | 5 | M, T |
| 0.1146 | 4 | α |
| 0.1125 | 3 | α |
| 0.1098 | 5 | α |
| 0.1078 | 5 | α |
| 0.1041 | 16 | α |
| 0.0997 | 12 | α |
| 0.0980 | 4 | α |
| 0.0907 | 7 | α |
| 0.0905 | 9 | α |

*α = Alpha alumina, T = tetragonal zirconia, M = monoclinic zirconia.

The average t-$ZrO_2$ crystal size in all the calcined powders was much smaller than the critical size [8] needed for its stabilization at room temperature (Table III). Therefore, it is speculated that the t-$ZrO_2$ → m-$ZrO_2$ transformation observed in the Procedure III powder (after DTA) and the 1550° C heated and annealed Procedure I powder was related more significantly to strain energy [29] and/or some unknown chemical effects [30, 31] than to the surface energy [30, 32].

## 4. Conclusions

1. $80Al_2O_3 \cdot 20ZrO_2$ (wt %) powders were synthesized by three processes based on three different chemical principles; namely, the chemical polymerization process, the process based on the destabilization of mixed sols, and the coprecipitation process. The elementary particles produced by these processes were of the order of 1.5 to 3.0 nm and were amorphous to electron diffraction.

2. Significant differences in the weight loss and thermal characteristics, surface area, and pore structures where observed among the powders are related to their synthesis chemistry.

3. On heat treatment, the net change of the pore structure of the powders varied due to the differences in (a) the initial pore structure and (b) rates of pore closing and pore enlargement that occurred simultaneously.

4. The powders produced were of lower density, which might be due to their structural configurations. These powders could be fully densified at ~ 1200° C.

5. The chemistry of powder synthesis significantly influenced the crystallization behaviour of the powders.

6. The average alumina and zirconia crystal sizes in the calcined powders were in the 20 to 80 nm range.

7. The stability of the tetragonal phase of zirconia was influenced by the synthesis chemistry of the powders.

## Acknowledgements

The author thanks K. Bachman for assisting in the laboratory work; J. Orr and C. Minton for the work of scanning transmission microscopy; A. Skidmore and L. Muttart for the X-ray analyses; F. Buffington for determining the helium densities; Harrop Industries, Columbus, for DTA and TGA; and Qunatachrome Corp., New York, for the BET measurements. The work was performed as a part of the in-house sol–gel development activities at Battelle Columbus Division.

## References

1. N. CLAUSSEN and M. RÜHLE, in "Advances in Ceramics", Vol. 3, edited by A. H. Heuer and L. W. Hobbs (The American Ceramic Society Inc., Columbus, Ohio, 1981) p. 137.
2. N. CLAUSSEN, *J. Amer. Ceram. Soc.* **59** (1976) 49.
3. F. F. LANGE and D. J. GREEN, in "Advances in Ceramics", Vol. 3, edited by A. H. Heuer and L. W. Hobbs (The American Ceramic Society Inc., 1981) p. 217.
4. Y. MURASE, E. KATO and K. DIAMON, *J. Amer. Ceram. Soc.* **69** (1986) 83.
5. B. KIBBEL and A. H. HEUER, *ibid.* **69** (1986) 231.
6. R. STEVENS and P. A. EVANS, *Brit. Ceram. Trans. J.* **83** (1984) 2831.
7. D. J. GREEN, *J. Amer. Ceram. Soc.* **65** (1982) 610.
8. A. H. HEUER, N. CLAUSSEN, W. M. KRIVEN and M. RÜHLE, *ibid.* **65** (1982) 642.
9. M. RÜHLE, N. CLAUSSEN and A. H. HEUER, *ibid.* **69** (1986) 195.
10. S. R. WITEK and E. P. BUTLER, *ibid.* **69** (1986) 523.
11. D. W. SPROSON and G. L. MESSING, *ibid.* **67** (1984) C-92.
12. I. A. AKSAY, *ibid.* **66** (1983) C-190.
13. F. F. LANGE and M. M. HIRLINGER, *ibid.* **67** (1984) 164.
14. N. CLAUSEEN, *ibid.* **61** (1978) 85.
15. M. KAGAWA, M. KIKUCHI, Y. SYONO and T. NAGAE, *ibid.* **66** (1983) 751.
16. B. FEGLEY JR., P. WHITE and H. K. BOWEN, *ibid.* **68** (1985) C-60.
17. E. A. PUGAR and P. E. D. MORGAN, *ibid.* **69** (1986) C-120.
18. S. HORI, M. YOSHIMURA, S. SOMIYA, R. KWITA and H. KAJI, *J. Mater. Sci. Lett.* **4** (1985) 413.
19. J. ECHIGOYA, Y. TAKABAYACHI and H. SUTO, *ibid.* **5** (1986) 153.
20. L. MAZEROLLES, D. MICHEL and R. PORTIER, *J. Amer. Ceram. Soc.* **69** (1986) 252.

21. J. C. DEBSIKDAR, *J. Mater. Sci.* **20** (1985) 4454.
22. J. C. DEBSIKDAR, *J. Non-Cryst. Solids* **86** (1986) 231.
23. M. E. A. HERMANS, *Powder Metallurgy International* **6** (1973) 137.
24. S. P. MUKHERJEE, J. C. DEBSIKDAR and T. L. BEAM, "Ultrapure Glass Optical Waveguide Development in Microgravity by the Sol-Gel Process", Draft Final Report to Jet Propulsion Laboratory (Contract No. 955710), January 15, 1982 (Battelle Columbus Laboratories, Columbus, Ohio).
25. S. KONDO, F. FUJIWARA and M. MUROYA, *J. Coll. Int. Sci.* **55** (1976) 421.
26. J. C. DEBSIKDAR, M. R. PASCUCCI, H. R. MURALIDHARA and R. R. WILLS, "Exploratory Development of Fused Silica Laser Windows", AFWL, Kirtland Air Force Base Final Report (Contract F-33615-82-C5004), February 25, 1985.
27. C. J. BRINKER, G. W. SCHERER and E. P. ROTH, *J. Non-Cryst. Solids* **72** (1985) 345.
28. B. E. YOLDAS, *ibid.* **63** (1984) 145.
29. D. L. PORTER, A. G. EVANS and A. H. HEUER, *Acta Metall.* **27** (1979) 1649.
30. R. C. GARVIE, *J. Phys. Chem.* **69** (1965) 1238.
31. Y. MURASE and E. KATO, *J. Amer. Ceram. Soc.* **62** (1979) 527.
32. R. C. GARVIE, *J. Phys. Chem.* **82** (1978) 218.

*Received 11 August*
*and accepted 23 September 1986*